ACS MEASUREMENT SCIENCE Au
AN OPEN ACCESS JOURNAL OF THE AMERICAN CHEMICAL SOCIETY

pubs.acs.org/measureau

Article

Automated Measurement of Electrogenerated Redox Species Degradation Using Multiplexed Interdigitated Electrode Arrays

Michael A. Pence, Oliver Rodríguez, Nikita G. Lukhanin, Charles M. Schroeder, and Joaquín Rodríguez-López*

Cite This: *ACS Meas. Sci. Au* 2023, 3, 62–72

Read Online

ACCESS | Metrics & More | Article Recommendations | Supporting Information

ABSTRACT: Characterizing the decomposition of electrogenerated species in solution is essential for applications involving electrosynthesis, homogeneous electrocatalysis, and energy storage with redox flow batteries. In this work, we present an automated, multiplexed, and highly robust platform for determining the rate constant of chemical reaction steps following electron transfer, known as the EC mechanism. We developed a generation-collection methodology based on microfabricated interdigitated electrode arrays (IDAs) with variable gap widths on a single device. Using a combination of finite-element simulations and statistical analysis of experimental data, our results show that the natural logarithm of collection efficiency is linear with respect to gap width, and this quantitative analysis is used to determine the decomposition rate constant of the electrogenerated species (k_c). The integrated IDA method is used in a series of experiments to measure k_c values between ~0.01 and 100 s^{-1} in aqueous and nonaqueous solvents and at concentrations as high as 0.5 M of the redox-active species, conditions that are challenging to address using standard methods based on conventional macroelectrodes. The versatility of our approach allows for characterization of a wide range of reactions including intermolecular cyclization, hydrolysis, and the decomposition of candidate molecules for redox flow batteries at variable concentration and water content. Overall, this new experimental platform presents a straightforward automated method to assess the degradation of redox species in solution with sufficient flexibility to enable high-throughput workflows.

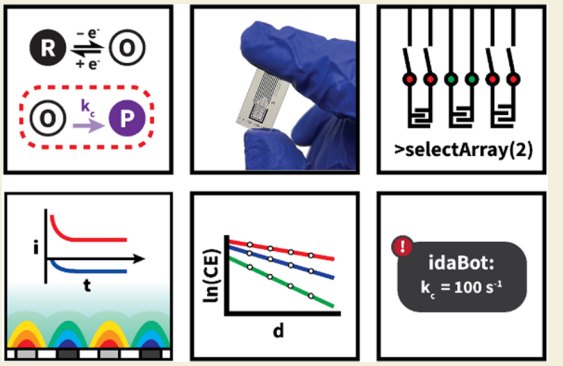

KEYWORDS: *Automation, microfabrication, interdigitated arrays, electrochemical analysis, EC mechanism, redox flow batteries*

INTRODUCTION

Electron transfer reactions at electrodes often generate species that undergo chemical reactions within the electrolyte, such as the EC mechanism where E denotes an electrochemical step and C a chemical reaction step. These types of reactions are essential for applications involving electrosynthesis and molecular electrocatalysis, where the subsequent reaction steps generate a product of interest.[1−3] Conversely, in systems such as redox flow batteries, downstream reactions often decrease the device performance through irreversible charge capacity losses, which limits the lifetime of the device.[4−7] In both cases, understanding the kinetics of the subsequent reaction steps is critical to allow for parameter tuning for enhanced performance. Common electrochemical techniques such as cyclic voltammetry (CV) and chronoamperometry are widely used to determine the characteristic time of these chemical steps. For instance, in CV using a single working electrode, the ratio of the return to forward wave peak intensity is typically measured, and this ratio is related to the half-life of the product of interest. However, CV often faces difficulties in measuring rapid steps because the characteristic reaction times are linked to the scan rate. Although the use of high-speed electronics[8−11] improves the performance of these transient techniques, these methods suffer fundamental limitations that increase with the scan rate such as double-layer charging and uncompensated resistance.

To overcome the potential pitfalls that accompany transient electrochemical measurement techniques, generation-collection strategies are often used.[12,13] Generation-collection methods rely on a bipotentiostat that controls two working electrodes: a generator that produces the redox active species, and a collector on which a suitable potential is applied to revert the redox reaction occurring at the generator.[14−23] The ratio of collector to generator currents gives a collection efficiency (CE) that is calibrated to account for losses due to mass transport between electrodes and therefore reports on nature of the chemical reactions. The generation-collection strategy

Received: September 12, 2022
Revised: October 14, 2022
Accepted: October 18, 2022
Published: November 1, 2022

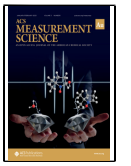

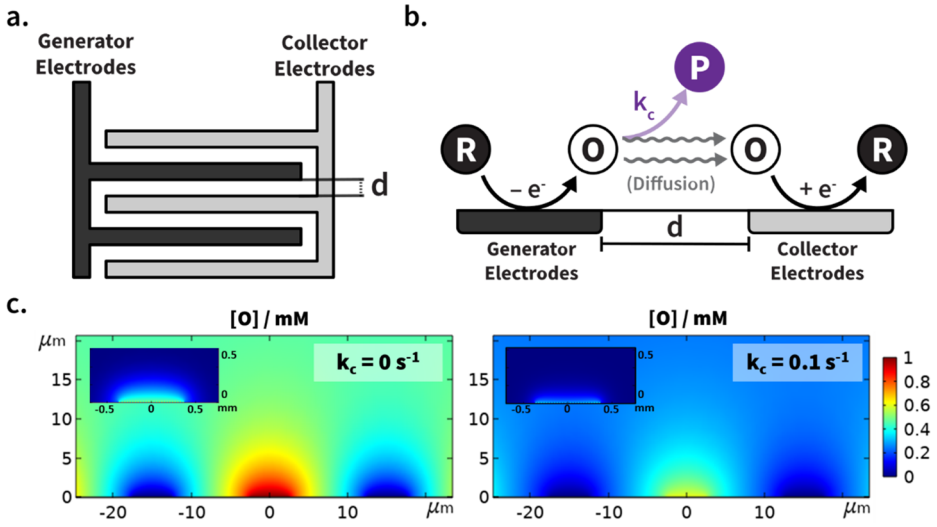

Figure 1. Workflow for a generation-collection experiment using interdigitated electrode arrays (IDAs). (a) Schematic showing top-down view of the IDA geometry. (b) Working schematic (side view) of generation-collection at an IDA for the reaction R ⇌ O → P, with k_c, the rate constant for the irreversible chemical decomposition step and gap width d. (c) Concentration profiles of species O in the absence and presence of a chemical reaction with a constant gap width focusing on the electrode surface (side view). Inset shows the zoomed-out concentration profile of O on the entire simulation space. All simulations use a constant electrode width of 5 μm. Concentration of O ranges from 0 mM (blue) to 1 mM (red).

for kinetic analysis of subsequent reaction steps is realized most commonly with instruments such as the rotating-ring-disk electrode (RRDE)[24] and the scanning electrochemical microscope (SECM).[25−27] In these techniques, diffusional time-of-flight is controlled by mechanical means by adjusting the rotation rate (ω) or the tip-to-substrate distance (d), respectively. The extent to which a chemical reaction occurs is determined by analyzing the change in CE as the time-of-flight of the electrogenerated species is varied. In particular for the SECM, the characteristic time is approximated by the diffusional time $t = d^2/D$, where D is the diffusion coefficient of the species. Here, t is controlled by means of an approach curve, where the CE is measured at a decreasing series of tip−substrate distances. For these methods, the strategy generally consists of multiple generation-collection experiments performed over a range of diffusional time-of-flights, thereby enabling the CE versus d curve to be analyzed to determine the corresponding chemical kinetics. Despite the utility of SECM and related methods, these techniques often require large sample volumes and mechanical control of instrumentation, which can complicate automation for high-throughput analysis.[28,29]

Another generation-collection method consists of using microfabricated devices based on interdigitated electrode arrays (IDAs). The IDA electrode geometry has been used in a range of applications involving electrochemical biosensing, with many applications taking advantage of its high collection efficiencies and possibility for miniaturization.[30−37] It consists of two interdigitated arrays of microband electrodes with a consistent interelectrode gap width (Figure 1a). Generation-collection experiments are performed with the two electrodes, and the diffusional time-of-flight is set by the gap width. As shown in Figure 1b, the generator electrode oxidizes R and forms the electrochemically active species O, which can undergo a subsequent chemical reaction with a rate constant of k_c, forming the electrochemically inactive product P. Any remaining species will be rereduced at the collector electrode back into species R. Degradation of electrogenerated O into the inactive product P will lead to decreased CE. Figure 1c shows a simulated concentration profile of species O for the type of IDA devices studied here and described in detail below, illustrating how k_c leads to a depleted profile compared to the purely diffusional case with no decomposition.

IDAs have been used sporadically to measure chemical reaction rates, though quantitative analysis of experimental data generally requires complementary modeling and simulations. The need for computational modeling is impractical for real-time automated determination of rate constants considering the expensive computational time required for 2D transport simulations with complex geometries.[38] Moreover, these methods rely on fitting to CV data, which are susceptible to distortions arising from sluggish charge transfer kinetics or uncompensated solution resistance. However, a few examples provide a glimpse of their quantitative power; recently gap width variation has been explored by using arrays of individually addressable microband electrodes as a platform to distinguish between individual catecholamines.[39]

In this work, we report the development of microfabricated multiplexed IDAs that overcome the limitations imposed by traditional generator-collector methods. The multiplexed IDA device incorporates a high CE geometry and a comprehensive model to determine chemical kinetics for the EC mechanisms. Using our multiplexed IDA method, time-of-flight is non-mechanically adjusted, which allows for facile automation and analysis. We demonstrate the robustness of the device by showing fabrication processes that can handle harsh oxidative cleaning and organic solvents. We further determined the rate constant for chemical reaction steps following electron transfer at the electrode surface, and generation-collection experiments are performed at four different gap widths on a single device. Our results show a linear relationship between the logarithm of CE and the interelectrode gap width, which remains highly linear even at relatively high concentrations of redox species. Finally, we implement our methodology on redox flow battery solutions and describe how automation will enable high-throughput experimentation based on these measurements.

https://doi.org/10.1021/acsmeasuresciau.2c00054
ACS Meas. Sci. Au 2023, 3, 62−72

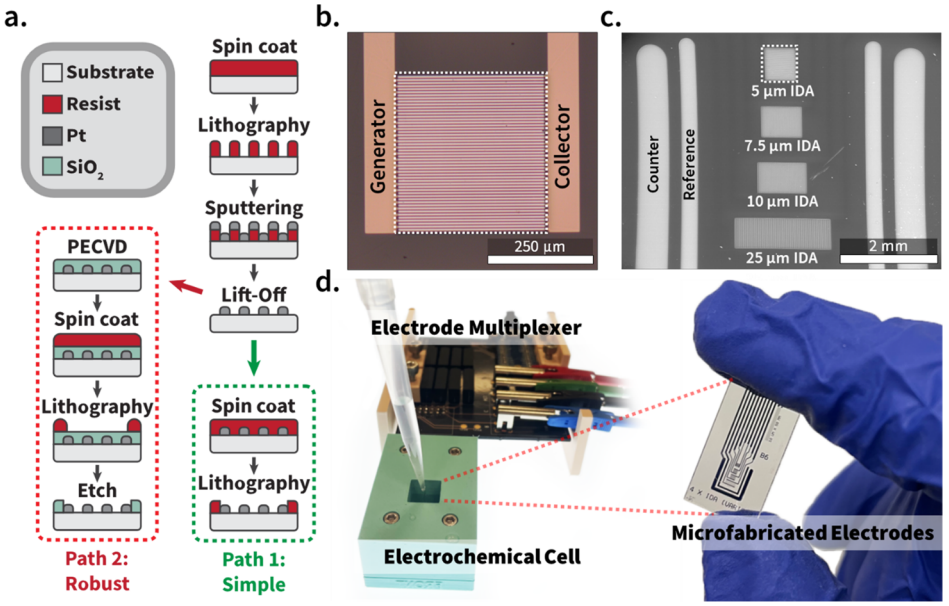

Figure 2. Fabrication process and images of the microfabricated devices and peripheral hardware. (a) Process for microfabrication of the device, including two alternative paths depending on experimental needs. (b) Optical micrograph of an IDA with a gap width of 5 μm. (c) SEM micrograph of IDAs with variable gap width as well as the counter and reference electrodes. (d) Image of the full device including microfabricated electrodes, electrochemical cell, and electrode multiplexer.

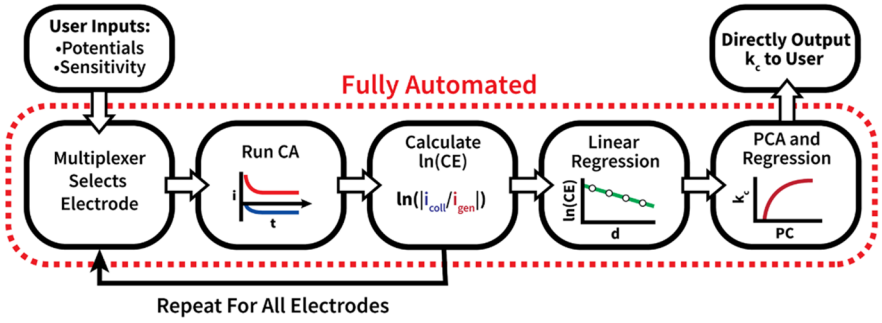

Figure 3. Flowchart depicting the electrochemical routine used to determine the rate constant for the chemical step. The red dotted line indicates the fully automated portions of the routine.

EXPERIMENTAL SECTION

Chemicals and Materials

All chemicals used in fabrication including SU8 2002 and KMPR 1010 photoresists, SU8 developer, and Omnicoat adhesion promoter were purchased from KayukaAM (Westborough, Massachusetts). Hydroxymethylferrocene (97%), *p*-aminophenol (98%), (±)-epinephrine hydrochloride (98%), and monobasic potassium phosphate (99%) were purchased from Sigma-Aldrich (St. Louis, Missouri). 85 w/w% phosphoric acid (ACS grade) was purchased from Fischer Chemical (Hampton, New Hampshire). Potassium nitrate (reagent grade) was purchased from VWR Life Sciences (Radnor, Pennsylvania). A 1,4-dimethyoxybenzene derivative (C7) was synthesized[40] and provided by the Zhang group from Argonne National Laboratory. A tri(dialkylamino)cyclopropenium derivative (HS-cyclopropenium) was synthesized[41] and provided by the Sanford group from the University of Michigan, Ann Arbor. Eighteen MΩ DI water was obtained from a Milli-Q purification system. All other chemicals were used as purchased without further purification. Glass slides (2" × 3") were purchased from Corning Inc. (Corning, New York). Anisotropically conductive film for making device connections was purchased from 3 M (St. Paul, Minnesota). Photomasks for the device were purchased from Front Range Photomasks (Phoenix, Arizona).

Device Design, Fabrication, and Packaging

Interdigitated arrays were fabricated on a 2" × 3" glass slide following the general process flow outlined in Figure 2a. Photolithography was used to define the electrode geometry as well as electrical connections. Substrates were sputtered with a 5 nm Ti adhesion layer followed by 100 nm of Pt, and a lift off procedure was performed. Insulated and exposed regions of the electrodes were defined by another photolithographic step, with either permanent photoresist (Path 1) or an oxide layer deposited through plasma-enhanced vapor deposition (PECVD) as the insulating material (Path 2). Additional details on device microfabrication are located in the Supporting Information (Supplemental Note S1). Fabricated substrates were diced into individual devices and bonded to a flexible ribbon cable with anisotropically conductive film. Prior to use, devices were cleaned for 2 min in a 100 W, 1 Torr oxygen plasma. Gap widths between the electrodes were obtained through optical microscopy. Figure 2b shows an optical micrograph of the 5 μm IDA, where the dotted white lines indicate the exposed electrode area. Figure 2c shows an electron micrograph of the four IDAs, as well as the integrated quasi-reference and counter electrodes.

Electrochemical Measurements

A CH Instruments model 760E bipotentiostat was used for all electrochemical measurements. All electrochemical experiments were performed in a custom designed electrochemical cell (Figure S2).

https://doi.org/10.1021/acsmeasuresciau.2c00054
ACS Meas. Sci. Au 2023, 3, 62−72

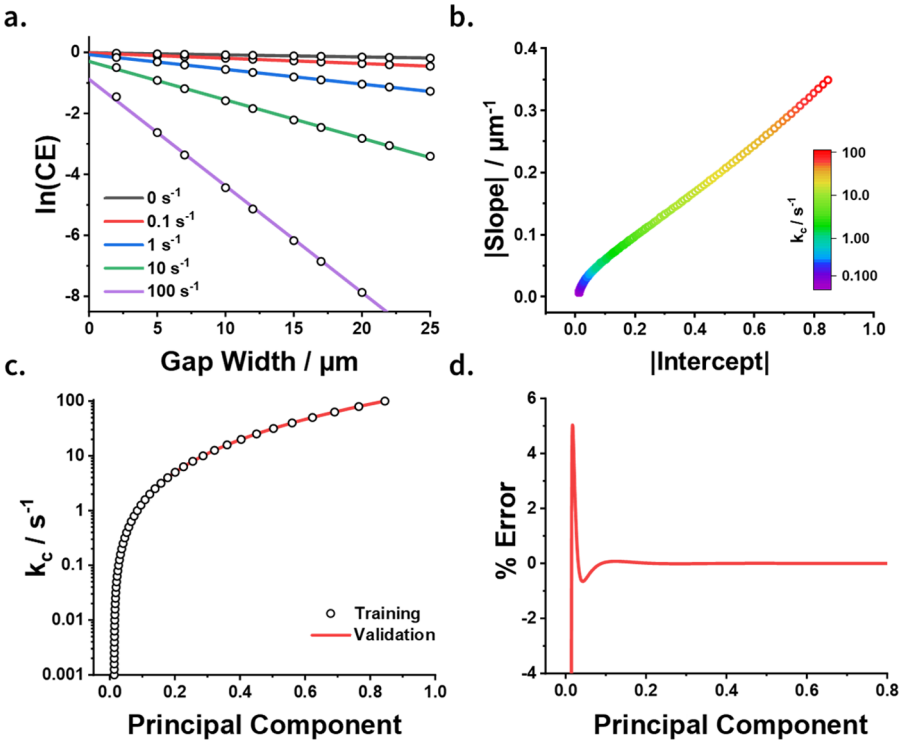

Figure 4. Determining chemical rate constants using simulations and principal component analysis of experimental data. (a) Plots of the natural logarithm of collection efficiency, ln(CE), versus gap width obtained by simulating EC mechanisms with different rate constants. (b) Plot depicting the relationship between the slopes and intercepts obtained for a range of k_c values. (c) Plot of reaction rate constant versus the first principal component. (d) Percent error in the measurement of k_c as a function of the first principal component.

Electrochemical pretreatment was performed prior to measurements by cycling electrodes in 0.1 M phosphate buffer solution (PBS) at pH 7.4 to clean any platinum oxide on the electrode surface (Figure S3). An external Ag/AgCl reference electrode was used to prevent shifts in potential during extensive cycling. Electrochemical measurements were performed using the integrated quasi-reference and counter electrodes, unless indicated otherwise. All electrochemical experiments were performed using a custom automated platform developed in our group that consists of the multiplexer (Figures 2d and S4) to select the IDA and a Python library that controls the multiplexer and the CHI760E bipotentiostat (Supplemental Note S2).

Simulation and Modeling

Simulations were performed using COMSOL Multiphysics 5.6 with the electrochemistry module. The 2D geometry consisted of an area of 2.5 × 2.5 mm^2, an out-of-plane thickness of 500 μm, and 51 lines that represented the electrode bars separated by a distance d (Figure S5). The mesh was created using the predefined normal distribution for the bulk of the solution and a free triangular meshing with a distribution of 50 elements around the electrodes (Figure S6). The out-of-plane thickness assumes that the electrode length is the same as the cell depth, meaning that each electrode finger would have an area of 5 × 500 μm^2 (Supporting Information).

Automation of Device Operation

The methodology presented in this work was developed with the goal of streamlining the characterization of redox-active species via automation. Our "plug-and-play" technique, in which minimal parameters and human interaction were needed to measure rate constants, is shown in Figure 3. Exploratory assessment of the system using traditional techniques such as CV permits the user to determine the initial inputs of generator potential, collector potential, and the expected current sensitivity. These initial input parameters are then fed into a script that runs all electrochemical experiments for each IDA size in a series fashion. A Python script includes commands to control the multiplexer, allowing for selection of a suitable IDA during runs, as well as to control the CHI760E bipotentiostat. The script also facilitates automated data analysis immediately after the experiments were performed, minimizing human error, ensuring repeatability, and providing prompt experimental feedback to inform experimental choices. The output of our workflow is the kinetic rate constant k_c, but the user can also access all files generated during analysis to qualitatively assess the data, if needed. This high level of abstraction requires only minimal electrochemical expertise for users to operate this device and methodology, without sacrificing the flexibility that advanced users might require to further explore functions in the device. To enable new users to efficiently use our technology, we include a sample Python script with instructions and a Jupyter notebook tutorial on how to develop and perform the principal component analysis and polynomial regression for nonspecialists (Supporting Information). Furthermore, the use of Python as a programming language allowed us to interface with third-party libraries not only for data analysis but also to communicate with the user remotely. For example, we have used a library to send remote notifications via a Slack account when the experiments were completed, including the determined values for k_c.

RESULTS AND DISCUSSION

Finite Element Simulations and Principal Component Analysis

We began by analyzing the EC mechanism using simulations and modeling of a first-order chemical reaction and Nernstian electrode kinetics. The chronoamperometric response of IDAs of 10 different gap widths ranging from 2 up to 25 μm were simulated for a range of chemical rate constants (k_c) between k_c = 0 (purely diffusional case with no chemical reaction step) and k_c = 1000 s^{-1} (Figure S7). The generator and collector electrodes were set to potentials recreating diffusion-limited oxidation and reduction, such that 0.5 and −0.5 V vs E^0, respectively. The current was then sampled at 30 s, longer than

https://doi.org/10.1021/acsmeasuresciau.2c00054
ACS Meas. Sci. Au 2023, 3, 62−72

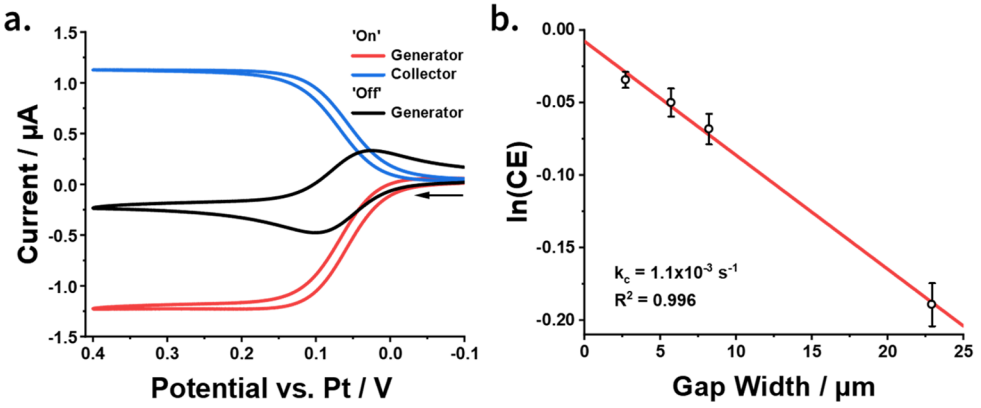

Figure 5. Electrochemical characterization of the fabricated IDAs in 1 mM FcMeOH with 100 mM KNO_3 as supporting electrolyte. (a) CV scans at the IDA with the smallest gap width in both single mode "off" and dual mode "on" and a scan rate of 0.1 V s^{-1}. (b) Plot of the natural logarithm of collection efficiency versus gap width sampled at 30 s.

the characteristic time scale for diffusion to reach steady state. We then determined the collection efficiency, defined as CE = $|i_{col}/i_{gen}|$, as a function of gap width. Our results show a decrease in collection efficiency as the gap width increases (Figure 4a), consistent with the diffusional loss of the electrogenerated species into the bulk solution. However, in all cases, efficiencies larger than 90% were achieved due to the small interelectrode gap width. The presence of a subsequent chemical reaction following electron transfer further decreases CE due to the consumption of the electrogenerated species by the chemical reaction. Importantly, we observe a linear relationship between the natural logarithm of the collection efficiency and the IDA gap width, at all chemical rate constants used, as shown in Figure 4a. For the geometry and conditions used in these experiments (Supporting Information), this observation dramatically simplifies the analysis of the experimental rate constants.

Our results show that, as the value of k_c increases, the slope of plots of CE versus d become steeper and the intercept becomes more negative (Figures S8 and S9), suggesting that these parameters can be used in a linear regression model to predict k_c. However, plotting intercept against slope as shown in Figure 4b reveals an underlying correlation, implying that one parameter can be used to predict the other. To address this observation, we performed dimensionality reduction using principal component analysis (PCA). Here, the data are first normalized to achieve a zero mean and unit variance respectively, which facilitates data analysis. Reducing the data to a single component yielded an explained variance ratio of 99.8%, ensuring that most of the variation can be represented by the first principal component (PC). In this way, a plot of the first PC versus k_c can be used to estimate chemical rate constants; a suitable equation describing this relation was found to be a fifth-order polynomial (Figure S10). Figure 4c and d shows the results from PCA as well as the error in determining k_c, defined as

$$\%\ \text{error} = (1 - k_c^{\text{pred}}/k_c^{\text{real}}) \times 100\% \quad (1)$$

The error abruptly increases for values of $k_c < 1 \times 10^{-2}$ s^{-1}, which we take as the lower bound for chemical rate constants that can be determined using this methodology. On the other hand, the largest rate constant that can be accurately measured is $\approx 1 \times 10^{2}$ s^{-1} based on our estimation of measurable collection current at typical (<1 M) redox-active concentrations and for the gap width values explored here. Faster or slower chemical rates can be obtained with alternative interelectrode separations, assuming that the steady-state condition in the generation/collection process is fulfilled. Based on results from simulations, we determined that our methodology is insensitive to diffusion coefficient (Figure S12) and that it can be used with any distance separations, provided the bar length representing the electrode has a high aspect ratio compared to its width (500 versus 5 μm, respectively). All results in this work use the intercept and slope of the ln(CE) versus gap width curve to determine k_c through PCA and polynomial regression. In the following sections, we demonstrate this methodology with a variety of reactions to highlight its general applicability.

Electrochemical Measurements in the Absence of a Chemical Reaction

We first tested the device with a solution of 1 mM hydroxymethylferrocene (FcMeOH) in 100 mM KNO_3 supporting electrolyte, which is a well-known redox species that displays reversible electrochemistry and no appreciable decomposition in the time scale of typical CV experiments. While we are not aware of a measured decomposition rate for FcMeOH, similar derivatives such as (ferrocenylmethyl)-trimethylammonium chloride are known to decay by 1.85% per day (2.2×10^{-7} s^{-1}) in the charged state.[42] In the absence of a chemical reaction, the collection efficiency solely reflects the diffusional loss of electrogenerated species into bulk solution. CV was performed with the selected generator electrode sweeping from −0.1 to 0.4 V at a scan rate of 0.1 V s^{-1}. We first performed an experiment with the collector electrode at open circuit ("off") and then with the collector electrode held at −0.1 V ("on"), as shown in Figure 5a. Additional electrochemical results for FcMeOH and IDA gap widths are shown in Figure S14.

Evaluation of FcMeOH using the IDA displayed the expected behavior for the diffusional case. Figure 5a shows the CV behavior of the smallest gap width IDA. When the collector is off, the overlapping diffusion fields at the closely spaced IDA fingers create conditions for the array to act as a macroscopic electrode. Thus, at these scan rates, the response is characteristic of a linear diffusion profile with forward and reverse peaks. In contrast, when the collector electrode is held at a potential where diffusion limited reduction of $FcMeOH^+$ is expected, steady-state behavior with characteristic sigmoidal

https://doi.org/10.1021/acsmeasuresciau.2c00054
ACS Meas. Sci. Au 2023, 3, 62−72

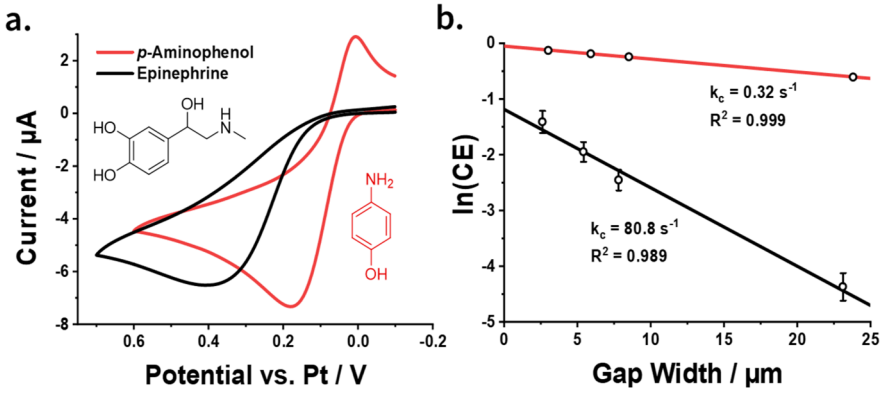

Figure 6. Characterization of aqueous redox mediators that undergo a chemical reaction following electrochemical oxidation. (a) CV scans at 0.1 V s^{-1} of 10 mM *p*-aminophenol and 10 mM epinephrine at the smallest gap width IDA. (b) Plot of ln(CE) vs gap width obtained at 15 s with chronoamperometry for both species. The error bars for the *p*-aminophenol plot are not visible at the given scale.

waves at both the generator and collector electrodes are observed. A redox cycling phenomenon,[43] analogous to positive feedback in SECM experiments, manifests as a significant increase in current at both electrodes when the collector is on. The current intensity due to the redox cycling phenomenon increases as the gap width is decreased. Figure 5b shows the characteristic linear relationship of the natural logarithm of collection efficiency, ln(CE), versus the gap width, as predicted by the simulations shown in Figure 4. The line of best fit has a slope of $-7.9 \times 10^{-3} \pm 5 \times 10^{-4}$ μm^{-1} and an intercept of $-7 \times 10^{-3} \pm 6 \times 10^{-3}$. Application of the PCA and polynomial regression model to these results yielded rate constants of 1×10^{-3} $s^{-1} \pm 8 \times 10^{-3}$ s^{-1} ($N = 7$). However, the slope and intercept are close to the simulated values for the purely diffusional case of -6.9×10^{-3} μm^{-1} and -1.1×10^{-2}, respectively, and the simulation model predicts that our system significantly loses sensitivity below $k_c < 1 \times 10^{-2}$ s^{-1} (Figure S8). Thus, the large experimental error in the determined value for k_c is consistent with the inability of our methodology to reliably report on its value for this well-known chemically stable redox system. While FcMeOH displayed characteristics closely resembling an unreactive, purely diffusional case, below we present several systems exhibiting measurable values of k_c.

Evaluating the Methodology on Aqueous Reactions

We now turn to the kinetically sensitive regime for IDA operation. Here, we studied reactions involving epinephrine and *p*-aminophenol, both of which are reported to undergo chemical reactions following electrochemical oxidation. Oxidation of epinephrine is followed by an irreversible intracyclization reaction, which has been reported to occur with an apparent rate constant of 87 s^{-1} in pH 7.4 solution.[44] For these experiments, we prepared a solution of 10 mM epinephrine in 0.1 M PBS at pH 7.4. CV was performed to select the appropriate generator and collector electrode potentials of 0.7 and −0.1 V, respectively. Similarly, *p*-aminophenol is electrochemically oxidized to *p*-benzoquinone imine, which undergoes an irreversible hydrolysis step to form benzoquinone. This hydrolysis step is reported to have a rate constant of 0.15 s^{-1} at pH 2.4.[45,46] For these experiments, we prepared a solution of 10 mM *p*-aminophenol in 0.1 M PBS at pH 2.4. Chronoamperometry was performed with the generator electrode held at 0.6 V and the collector electrode at −0.1 V. The collection efficiency for both systems was calculated as previously described, however the currents were sampled at 15 s to avoid the possibility of electrode fouling. IDA dimensions and additional electrochemical results for epinephrine and *p*-aminophenol are shown in Figures S15 and S16, respectively.

Our IDA devices successfully measured values of k_c with good agreement to previously reported results for reactions with rates that differ by 3 orders of magnitude. Figure 6a shows the chemical structures and CVs of epinephrine and *p*-aminophenol, measured at the smallest gap width IDA at a scan rate of 0.1 V s^{-1}. Qualitatively, the difference in rates for the chemical reactions are noted by the presence of a small peak upon the return sweep for *p*-aminophenol, but no return peak for epinephrine. The difference in rates is further shown in the ln(CE) versus gap width plot in Figure 6b, where the epinephrine data shows a significantly steeper slope with a more negative intercept than *p*-aminophenol. The line of best fit for epinephrine had a slope of -0.14 μm^{-1} and an intercept of −1.19, which yields an average observed rate constant of 80.8 ± 13.8 s^{-1}. The observed rate constant measured using our multiplexed IDA method was within the range of 87 ± 10 s^{-1} reported in prior literature.[44] *p*-Aminophenol yielded a slope of -2.3×10^{-2} μm^{-1} and an intercept of -5.0×10^{-2}, giving a rate constant of 0.32 ± 0.02 s^{-1}. The rate constant obtained for *p*-aminophenol is also similar to the reported value in literature[45,46] of 0.15 s^{-1}, within a factor of 2. It is possible that variation from previously reported results arise due to increased error in the model that is present at lower rate constants or due to electrode fouling. However, the linear response reflected in the results in Figure 6b is derived from the independent operation of four multiplexed electrode pairs, each operating with different characteristic times, which suggests that the IDA method yields precise measurements of kinetic rate constants.

Robustness of the Device

Fouling of the electrode surface through unwanted side reactions is a source of concern when carrying out repetitive measurements and when considering the long-term robustness of the device. Unwanted polymerization reactions of small organic molecules can occur upon electron transfer, forming films that are detrimental to electrode behavior. When chronoamperometry was performed on *p*-aminophenol for longer than 15 s, a rapid decrease in current at both generator and collector electrodes was observed (Figure S17). We attribute this behavior to fouling of the electrode surface by a film of poly-*p*-aminophenol.[47] Surface fouling on planar macroscopic electrodes used typically in electroanalysis is

https://doi.org/10.1021/acsmeasuresciau.2c00054
ACS Meas. Sci. Au 2023, 3, 62−72

often dealt with by polishing in between runs. However, polishing is not feasible at microfabricated electrodes, as the mechanical abrasion can destroy patterned electrodes. To circumvent these issues, we used oxygen plasma cleaning to remove any films formed on the electrode surface.[48] Plasma treatment was followed by aforementioned electrochemical cycling to reduce any formed oxide layer. The results in Figure 6 were obtained following this procedure for each run, but to demonstrate its effectiveness, the impact of the cleaning procedure is shown in Figure 7, where a surface film of poly-*p*-

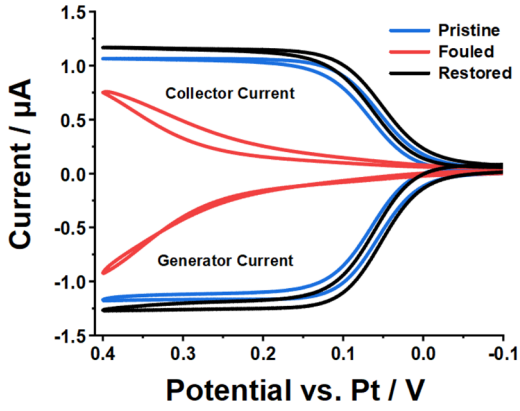

Figure 7. CVs of FcMeOH on a pristine device (blue), the device after significant fouling from *p*-aminophenol oxidation (red), and the device after oxygen plasma treatment and electrochemical cycling (black).

aminophenol significantly deteriorates the CV response of FcMeOH. In contrast, after 5 min of oxygen plasma treatment on the electrode, the film was removed and the reactivity of this redox species was observed on the device nearly indistinguishably to the pristine electrode.

To determine whether oxidative treatment on the electrodes may have a deteriorating effect on the photoresist insulator for electrodes fabricated using Path 1 in Figure 2a, we fabricated devices using a 1 μm thick SiO_2 insulating layer to prevent degradation during prolonged exposure (Path 2 in Figure 2a and Supporting Information). In addition to improved resistance against reactive etching by plasma, the SiO_2 layer does not swell or delaminate in organic solvents, which makes it ideal for characterizing nonaqueous systems as described in the following section.

Systematic Degradation Studies of Redox Flow Battery Electrolytes

In redox flow batteries, the highly resistive electrolyte solution and high concentrations of redox active species create substantial *iR* drop distortions when using transient characterization methods. Moreover, for nonaqueous flow battery electrolytes, our SiO_2 devices provide the opportunity to measure relevant properties without concerns on device stability. We therefore sought to characterize electrochemical behavior in organic nonaqueous systems using our integrated IDA measurement methodology. We performed a series of experiments by varying concentration and water content for two redox flow battery electrolytes, including an alkoxybenzene derivative from Argonne National Lab known as C7, and a cyclopropenium derivative known as HS-CP from University of Michigan Ann Arbor. The high oxidation potential of these species make them a prime candidate for use in redox flow batteries, but the large oxidation potential comes at a trade-off of increased reactivity of the oxidized form, which can react with chemical species such as water.[49] We studied the electrochemical behavior of both catholyte species outside of a drybox, at various concentrations of catholyte and water. For these experiments, we only used three devices over the course of the 48 experimental trials owing to the robustness of the SiO_2 insulated devices.

Redox flow batteries must operate with high concentrations of electroactive species, which necessitates the use of practical kinetic studies to be performed under similar conditions. The need to perform experiments at high concentrations poses major difficulties when performing typical CV measurements with a macroelectrode, as the resulting high currents greatly exacerbate the effects of *iR* drop in nonaqueous media.[50] Our device has an electrode area of 1.28×10^{-3} cm^2, 25 times smaller than that of a common 2 mm macrodisk electrode. The decreased area significantly lowers the measured current, making experiments at high concentrations more straightforward to perform. In Figure 8a and b, CV scans are shown at the generator electrodes for an ~5 μm gap width IDA for both the HS-CP and C7 catholytes at concentrations of 25 and 500 mM, with 1 M $TBAPF_6$ supporting electrolyte in acetonitrile. The smaller normalized current intensity at higher concentration of catholyte is due to a decreased diffusion coefficient of the species as the solution viscosity increases. For instance, for C7 solutions, the viscosity of a 25 mM solution is 1.13 cP, but it rises to 3.59 cP at 250 mM concentration. Although increased peak splitting due to *iR* drop is seen at the highest concentration of 500 mM, this measurement would be impractical for typical scan rate studies needed in transient CV at a macroelectrode and their resulting high currents. Furthermore, the distortion of the CV response does not affect our determination of k_c, as long as the generator and collector are poised to potentials ensuring mass transfer limited conditions during their operation. The indifference of our method to distortions of the CV response presents an advantage over transient CV methods for which wave shape distortions significantly hamper attempts to fit parameters, for instance, using digital simulations. Figure 8c shows the dependence of k_c with respect to redox-active species concentration. A notable aspect of the experiments at high concentrations is that the ln(CE) versus gap width plot was highly linear (Supporting Information), which highlights the robustness of our methodology. For both HS-CP and C7, no particular trend for k_c was identified as a function of concentration. The lack of dependence of rate on catholyte concentration suggests that possible radical−radical interactions of the electrogenerated radical cations either do not happen at a measurable time scale or do not have an obvious deleterious impact on their reactivity. The results obtained from these experiments are highly informative for scaling up to practical concentrations in a redox flow battery.[41]

A systematic study of the effect of water content on the observed rate constant was also carried out for both species, as shown in Figure 8d. HS-CP showed low sensitivity to the increasing presence of water, with degradation rates in the range of 0.05−0.14 s^{-1}. In contrast, the C7 species showed a marked increase in observed rate constant with increased water content, ranging from a minimum rate of 0.16 s^{-1} at 0 v/v% water content to a maximum rate of 2.52 s^{-1} with 10 v/v% water content. We posit that the high sensitivity of C7 to water is due to a previously reported degradation pathway,[40] where

https://doi.org/10.1021/acsmeasuresciau.2c00054
ACS Meas. Sci. Au 2023, 3, 62−72

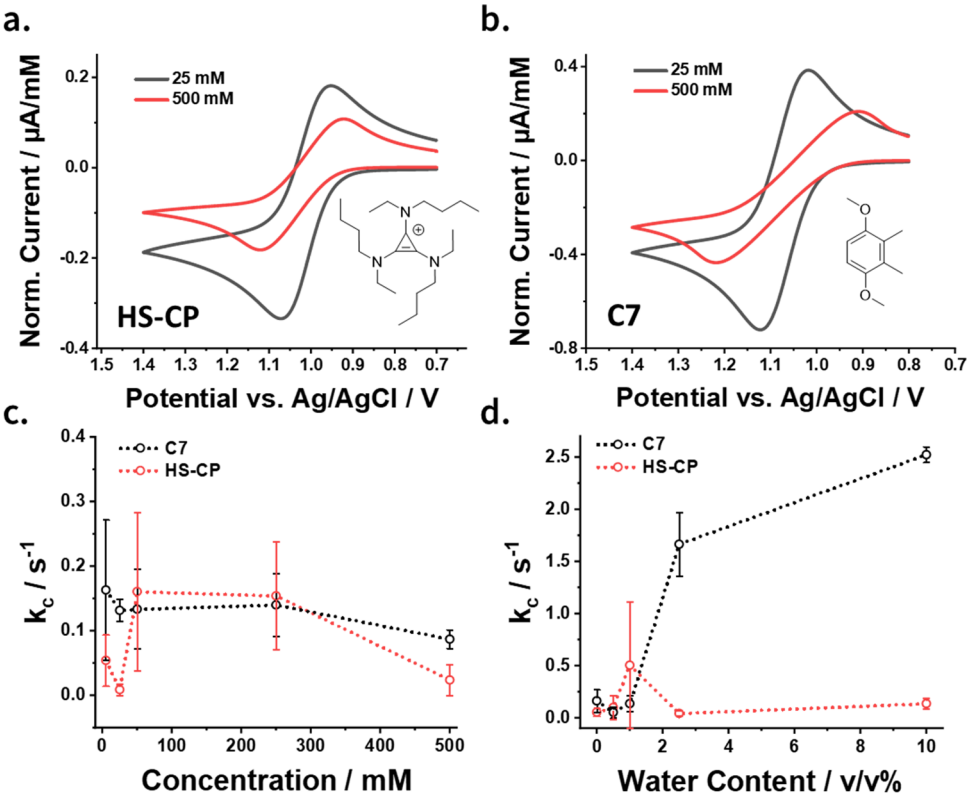

Figure 8. Electrochemical characterization of organic redox flow battery electrolytes. CV at a scan rate of 0.1 V s^{-1} of (a) HS-CP[41] and (b) C7,[40] both normalized by dividing the current by the concentration of the redox active species. (c) Observed rates for both species as a function of concentration. (d) Observed rates for both species at 5 mM concentration for each species with varied water content. For both HS-CP and C7, chronoamperometry was run with generator and collector electrode potentials at 1.4 and 0.7 V, respectively, with currents sampled at 15 s. To prevent potential shift of the integrated Pt quasi-reference at the higher concentrations, we used an external Ag/AgCl reference electrode with a salt bridge. IDA dimensions and additional electrochemical results for the C7 and HS-CP species are shown in Figures S18 and S19.

water can act as a nucleophile, causing the C7 molecule to undergo conversion into a quinone species. Although the rates observed at 0 v/v% water are larger than expected from reported cycling data,[40,41] it is important to note that these measurements are performed outside of the drybox, with a baseline level of water that is present even for the 0 v/v% data points.

Our IDA devices coupled to measurement automation are uniquely fitted to perform systematic studies exploring the impact of a variable, such as concentration or water content, on the stability of a redox system. As shown in Figure 7, a total of nine experiments were performed in triplicate for each catholyte species, requiring approximately 25 min each and a total experimental run time of 2 days. However, because the electrochemical experimentation and data analysis were fully automated, only ∼4 h was spent on actual hands-on experimental work, mostly dedicated to solution handling. From this view, the flexibility of our system is advantageous to design a fully autonomous device where decisions are made depending on certain conditions. For example, electrochemical cleaning can be automatically performed if electrode fouling is detected. Similarly, the system is be tasked with systematically deciding on variations of electrode potentials for exploratory work. Flexible operation of our device also allows for facile incorporation into other automated workflows, such as in chemical synthesis systems where a freshly prepared redox active material needs to be electrochemically characterized to measure degradation rates. Furthermore, several devices can be used in parallel enabling high-throughput experimentation, a direction our team is currently exploring. Overall, we believe that the robustness of our device, along with its flexibility for automated analysis makes it a powerful tool for electrochemists and nonelectrochemists alike.

CONCLUSION

In this work, we report the design and development of an electrochemical generation-collection device based on integrated, multiplexed IDAs at varying interelectrode gap width. We developed experimental methodology and data analysis for the device that enables the automated measurement of the rate constants of chemical processes following electrochemical reactions, i.e., the EC mechanism. Importantly, we discovered a linear dependence of the logarithm of collection efficiency versus interelectrode gap width, which dramatically simplified our analysis through the straightforward use of slope and intercept as inputs for our algorithm to elucidate the decomposition rate constants. We further introduced an optimized workflow for the use of the device which incorporates Python scripting to automate the multiplexing, data acquisition, and data analysis.

To demonstrate the versatility of our approach, we experimentally characterized a variety of redox-active species, in both aqueous and nonaqueous media. We measured rate constants over the range from ∼0.01 to 100 s^{-1}. Purely diffusive systems (i.e., with unmeasurable low rates of decomposition) such as a ferrocene derivative validated our simulations and the expected linear trend of ln(CE) versus gap

https://doi.org/10.1021/acsmeasuresciau.2c00054
ACS Meas. Sci. Au 2023, 3, 62−72

width. Measured rate constants for known chemical processes following electron transfer, such as the hydrolysis of *p*-aminophenol and the intramolecular cyclization of epinephrine, were in agreement with the literature. The robustness of our IDA devices was tested by removing organic passivating films using oxygen plasma cleaning and by introducing a modified fabrication process using SiO_2 instead of photoresist. The use of SiO_2 dramatically improves the resistance to delamination and swelling in nonaqueous media.

We further used our devices to characterize the chemical stability of redox-active species used in nonaqueous flow batteries as a demonstration of how our methodology can tackle technology relevant problems involving resistive and high concentration electrolytes. We performed systematic studies of organic redox flow battery electrolytes with C7 or HS-CP in acetonitrile, with concentrations up to 0.5 M of the electroactive species, and in the presence of water. Although redox-active concentration was not observed to impact the reactivity of either C7 or HS-CP, water notably impacted the rate of decomposition of electrogenerated C7 radical cations. Our automated methodology will enable users to gather mechanistic insight under conditions that would otherwise present overwhelming complications when performing typical scan-rate dependent studies with macroelectrodes. Moving forward, the automation of solution manipulation and dispensing can be incorporated into this instrumental framework. Automation will further minimize human error and allow users to perform extensive and systematic characterization of large sample libraries with minimal supervision. We envision that the ease of use and robustness of our method will enable users in a variety of fields including energy storage, electrosynthesis, and electrocatalysis among others to gain invaluable mechanistic insight that bolsters new discoveries in their investigations.

■ ASSOCIATED CONTENT

Supporting Information

The Supporting Information is available free of charge at https://pubs.acs.org/doi/10.1021/acsmeasuresciau.2c00054.

Additional fabrication, simulation, and experimental details (PDF)

Including 3D printable models for the electrochemical cell (STL), photomask design for a single IDA device (GDSII), sample python script to run an experiment (PY), Arduino code to control the multiplexer (INO), and Jupyter notebook tutorial for the data analysis methods (HTML) ZIP

■ AUTHOR INFORMATION

Corresponding Author

Joaquín Rodríguez-López − *Department of Chemistry, University of Illinois at Urbana—Champaign, Urbana, Illinois 61801, United States; Beckman Institute for Advanced Science and Technology, University of Illinois at Urbana—Champaign, Urbana, Illinois 61801, United States; Joint Center for Energy Storage Research (JCESR), Argonne National Laboratory, Lemont, Illinois 60439, United States;* orcid.org/0000-0003-4346-4668; Email: joaquinr@illinois.edu

Authors

Michael A. Pence − *Department of Chemistry, University of Illinois at Urbana—Champaign, Urbana, Illinois 61801, United States; Beckman Institute for Advanced Science and Technology, University of Illinois at Urbana—Champaign, Urbana, Illinois 61801, United States; Joint Center for Energy Storage Research (JCESR), Argonne National Laboratory, Lemont, Illinois 60439, United States;* orcid.org/0000-0001-5880-9812

Oliver Rodríguez − *Department of Chemistry, University of Illinois at Urbana—Champaign, Urbana, Illinois 61801, United States; Beckman Institute for Advanced Science and Technology, University of Illinois at Urbana—Champaign, Urbana, Illinois 61801, United States; Joint Center for Energy Storage Research (JCESR), Argonne National Laboratory, Lemont, Illinois 60439, United States;* orcid.org/0000-0003-2350-1214

Nikita G. Lukhanin − *Department of Chemistry, University of Illinois at Urbana—Champaign, Urbana, Illinois 61801, United States; Beckman Institute for Advanced Science and Technology, University of Illinois at Urbana—Champaign, Urbana, Illinois 61801, United States; Joint Center for Energy Storage Research (JCESR), Argonne National Laboratory, Lemont, Illinois 60439, United States*

Charles M. Schroeder − *Department of Chemical and Biomolecular Engineering, Department of Materials Science and Engineering, and Beckman Institute for Advanced Science and Technology, University of Illinois at Urbana—Champaign, Urbana, Illinois 61801, United States; Joint Center for Energy Storage Research (JCESR), Argonne National Laboratory, Lemont, Illinois 60439, United States;* orcid.org/0000-0001-6023-2274

Complete contact information is available at: https://pubs.acs.org/10.1021/acsmeasuresciau.2c00054

Author Contributions

CRediT: **Michael A. Pence** conceptualization (equal), data curation (equal), formal analysis (equal), investigation (lead), methodology (equal), visualization (equal), writing-original draft (equal); **Oliver Rodríguez** conceptualization (equal), formal analysis (equal), investigation (equal), methodology (equal), software (lead), validation (equal), visualization (equal), writing-original draft (equal); **Nikita G. Lukhanin** investigation (supporting), methodology (supporting), software (supporting), visualization (supporting); **Charles M. Schroeder** funding acquisition (equal), project administration (equal), resources (equal), supervision (equal), writing-review & editing (equal); **Joaquín Rodríguez-López** conceptualization (lead), funding acquisition (equal), project administration (lead), resources (equal), supervision (lead), writing-review & editing (equal).

Notes

The authors declare no competing financial interest.

■ ACKNOWLEDGMENTS

The research was financially supported by the Joint Center for Energy Storage Research (JCESR), an Energy Innovation Hub funded by the U.S. Department of Energy, Office of Science, Basic Energy Sciences. The material presented in this work was carried out in part in the Micro-Nano-Mechanical Systems Cleanroom Laboratory within the Department of Mechanical

Science and Engineering at the University of Illinois. We graciously acknowledge Dr. Jingjing Zhang and Dr. Lu Zhang from Argonne National Laboratory, and Dr. Yichao Yan and Dr. Melanie Sanford from University of Michigan at Ann Arbor for synthesizing and supplying us with redox flow battery materials to use. We thank Dr. Inkyu Oh for thoughtful discussions.

REFERENCES

(1) Danly, D. E. Development and Commercialization of the Monsanto Electrochemical Adiponitrile Process. *J. Electrochem. Soc.* **1984**, *131* (10), 435C.
(2) Zhang, W.; Lu, L.; Zhang, W.; Wang, Y.; Ware, S. D.; Mondragon, J.; Rein, J.; Strotman, N.; Lehnherr, D.; See, K. A.; Lin, S. Electrochemically Driven Cross-Electrophile Coupling of Alkyl Halides. *Nature* **2022**, *604* (7905), 292−297.
(3) Hamby, T. B.; LaLama, M. J.; Sevov, C. S. Controlling Ni Redox States by Dynamic Ligand Exchange for Electroreductive Csp3−Csp2 Coupling. *Science* **2022**, *376* (6591), 410−416.
(4) Yan, Y.; Vaid, T. P.; Sanford, M. S. Bis(Diisopropylamino)-Cyclopropenium-Arene Cations as High Oxidation Potential and High Stability Catholytes for Non-Aqueous Redox Flow Batteries. *J. Am. Chem. Soc.* **2020**, *142* (41), 17564−17571.
(5) Bheemireddy, S. R.; Li, Z.; Zhang, J.; Agarwal, G.; Robertson, L. A.; Shkrob, I. A.; Assary, R. S.; Zhang, Z.; Wei, X.; Cheng, L.; Zhang, L. Fluorination Enables Simultaneous Improvements of a Dialkoxybenzene-Based Redoxmer for Nonaqueous Redox Flow Batteries. *ACS Appl. Mater. Interfaces* **2022**, *14* (25), 28834−28841.
(6) Zhao, Y.; Yu, Z.; Robertson, L. A.; Zhang, J.; Shi, Z.; Bheemireddy, S. R.; Shkrob, I. A.; Y Z; Li, T.; Zhang, Z.; Cheng, L.; Zhang, L. Unexpected Electrochemical Behavior of an Anolyte Redoxmer in Flow Battery Electrolytes: Solvating Cations Help to Fight against the Thermodynamic−Kinetic Dilemma. *J. Mater. Chem. A* **2020**, *8* (27), 13470−13479.
(7) Yan, Y.; Robinson, S. G.; Vaid, T. P.; Sigman, M. S.; Sanford, M. S. Simultaneously Enhancing the Redox Potential and Stability of Multi-Redox Organic Catholytes by Incorporating Cyclopropenium Substituents. *J. Am. Chem. Soc.* **2021**, *143* (33), 13450−13459.
(8) Nicholson, R. S.; Shain, I. Theory of Stationary Electrode Polarography for a Chemical Reaction Coupled between Two Charge Transfers. *Anal. Chem.* **1965**, *37* (2), 178−190.
(9) Andrieux, C. P.; Hapiot, P.; Saveant, J. M. Fast Potential Step Techniques at Ultramicroelectrodes: Application to the Kinetic Characterization of Electrochemically Generated Short-Lived Species. *J. Phys. Chem.* **1988**, *92* (21), 5992−5995.
(10) Forster, R. J. Mechanism and Kinetics of Homogeneous 1-Methyl-Carbamidopyridinyl Radical Reactions. *Phys. Chem. Chem. Phys.* **1999**, *1* (7), 1543−1548.
(11) Amatore, C.; Maisonhaute, E. When Voltammetry Reaches Nanoseconds. *Anal. Chem.* **2005**, *77* (15), 303 A−311 A.
(12) McKenzie, E. C. R.; Hosseini, S.; Petro, A. G. C.; Rudman, K. K.; Gerroll, B. H. R.; Mubarak, M. S.; Baker, L. A.; Little, R. D. Versatile Tools for Understanding Electrosynthetic Mechanisms. *Chem. Rev.* **2022**, *122* (3), 3292−3335.
(13) Sandford, C.; Edwards, M. A.; Klunder, K. J.; Hickey, D. P.; Li, M.; Barman, K.; Sigman, M. S.; White, H. S.; Minteer, S. D. A Synthetic Chemist's Guide to Electroanalytical Tools for Studying Reaction Mechanisms. *Chem. Sci.* **2019**, *10* (26), 6404−6422.
(14) Frumkin, A.; Nekrasov, L.; Levich, B.; Ivanov, Ju. Die anwendung der rotierenden scheibenelektrode mit einem ringe zur untersuchung von zwischenprodukten elektrochemischer reaktionen. *J. Electroanal. Chem.* **1959**, *1* (1), 84−90.
(15) Fisher, A. C.; Compton, R. G. Double-Channel Electrodes: Homogeneous Kinetics and Collection Efficiency Measurements. *J. Appl. Electrochem.* **1991**, *21* (3), 208−212.
(16) Martin, R. D.; Unwin, P. R. Theory and Experiment for the Substrate Generation/Tip Collection Mode of the Scanning Electrochemical Microscope: Application as an Approach for Measuring the Diffusion Coefficient Ratio of a Redox Couple. *Anal. Chem.* **1998**, *70* (2), 276−284.
(17) Rajantie, H.; Strutwolf, J.; Williams, D. E. Theory and Practice of Electrochemical Titrations with Dual Microband Electrodes. *J. Electroanal. Chem.* **2001**, *500* (1), 108−120.
(18) Paixão, T. R. L. C.; Richter, E. M.; Brito-Neto, J. G. A.; Bertotti, M. The Use of a New Twin-Electrode Thin-Layer Cell to the Study of Homogeneous Processes Coupled to Electrode Reactions. *J. Electroanal. Chem.* **2006**, *596* (2), 101−108.
(19) Lewis, P. M.; Sheridan, L. B.; Gawley, R. E.; Fritsch, I. Signal Amplification in a Microchannel from Redox Cycling with Varied Electroactive Configurations of an Individually Addressable Microband Electrode Array. *Anal. Chem.* **2010**, *82* (5), 1659−1668.
(20) Anderson, M. J.; Crooks, R. M. High-Efficiency Generation-Collection Microelectrochemical Platform for Interrogating Electroactive Thin Films. *Anal. Chem.* **2014**, *86* (19), 9962−9969.
(21) Han, D.; Zaino, L. P.; Fu, K.; Bohn, P. W. Redox Cycling in Nanopore-Confined Recessed Dual-Ring Electrode Arrays. *J. Phys. Chem. C* **2016**, *120* (37), 20634−20641.
(22) Kostiuchenko, Z. A.; Lemay, S. G. Quasi-One-Dimensional Generator-Collector Electrochemistry in Nanochannels. *Anal. Chem.* **2020**, *92* (3), 2847−2852.
(23) Lotfi Marchoubeh, M.; Cobb, S. J.; Abrego Tello, M.; Hu, M.; Jaquins-Gerstl, A.; Robbins, E. M.; Macpherson, J. V.; Michael, A. C.; Fritsch, I. Miniaturized Probe on Polymer SU-8 with Array of Individually Addressable Microelectrodes for Electrochemical Analysis in Neural and Other Biological Tissues. *Anal. Bioanal. Chem.* **2021**, *413* (27), 6777−6791.
(24) Amatore, C.; Capobianco, G.; Farnia, G.; Sandona, G.; Saveant, J. M.; Severin, M. G.; Vianello, E. Kinetics and Mechanism of Self-Protonation Reactions in Organic Electrochemical Processes. *J. Am. Chem. Soc.* **1985**, *107* (7), 1815−1824.
(25) Unwin, P. R.; Bard, A. J. Scanning Electrochemical Microscopy. 9. Theory and Application of the Feedback Mode to the Measurement of Following Chemical Reaction Rates in Electrode Processes. *J. Phys. Chem.* **1991**, *95* (20), 7814−7824.
(26) Cannan, S.; Cervera, J.; Steliaros, R. J.; Bitziou, E.; Whitworth, A. L.; Unwin, P. R. Scanning Electrochemical Microscopy (SECM) Studies of Catalytic EC' Processes: Theory and Experiment for Feedback, Generation/Collection and Imaging Measurements. *Phys. Chem. Chem. Phys. PCCP* **2011**, *13* (12), 5403−5412.
(27) Zhou, F.; Unwin, P. R.; Bard, A. J. Scanning Electrochemical Microscopy. 16. Study of Second-Order Homogeneous Chemical Reactions via the Feedback and Generation/Collection Modes. *J. Phys. Chem.* **1992**, *96* (12), 4917−4924.
(28) Topalov, A. A.; Katsounaros, I.; Meier, J. C.; Klemm, S. O.; Mayrhofer, K. J. J. Development and Integration of a LabVIEW-Based Modular Architecture for Automated Execution of Electrochemical Catalyst Testing. *Rev. Sci. Instrum.* **2011**, *82* (11), 114103.
(29) Alden, S. E.; Siepser, N. P.; Patterson, J. A.; Jagdale, G. S.; Choi, M.; Baker, L. A. Array Microcell Method (AMCM) for Serial Electroanalysis. *ChemElectroChem.* **2020**, *7* (5), 1084−1091.
(30) Zaccheo, B. A.; Crooks, R. M. Detection of an Epstein−Barr Genome Analog at Physiological Concentrations via the Biometallization of Interdigitated Array Electrodes. *Anal. Chem.* **2009**, *81* (14), 5757−5761.
(31) Nishihara, H.; Dalton, F.; Murray, R. W. Interdigitated Array Electrode Diffusion Measurements in Donor/Acceptor Solutions in Polyether Electrolyte Solvents. *Anal. Chem.* **1991**, *63* (24), 2955−2960.
(32) Chidsey, C. E.; Feldman, B. J.; Lundgren, C.; Murray, R. W. Micrometer-Spaced Platinum Interdigitated Array Electrode: Fabrication, Theory, and Initial Use. *Anal. Chem.* **1986**, *58* (3), 601−607.
(33) Borchers, J. S.; Campbell, C. R.; Van Scoy, S. B.; Clark, M. J.; Anand, R. K. Redox Cycling at an Array of Interdigitated Bipolar Electrodes for Enhanced Sensitivity in Biosensing**. *ChemElectroChem.* **2021**, *8* (18), 3482−3491.
(34) Nepomnyashchii, A. B.; Kolesov, G.; Parkinson, B. A. Electrogenerated Chemiluminescence of BODIPY, Ru(Bpy)32+,

and 9,10-Diphenylanthracene Using Interdigitated Array Electrodes. *ACS Appl. Mater. Interfaces* **2013**, *5* (13), 5931−5936.
(35) Mathew, D. G.; Beekman, P.; Lemay, S. G.; Zuilhof, H.; Le Gac, S.; van der Wiel, W. G. Electrochemical Detection of Tumor-Derived Extracellular Vesicles on Nanointerdigitated Electrodes. *Nano Lett.* **2020**, *20* (2), 820−828.
(36) Feldman, B. J.; Feldberg, S. W.; Murray, R. W. An Electrochemical Time-of-Flight Experiment. *J. Phys. Chem.* **1987**, *91* (26), 6558−6560.
(37) Postlethwaite, T. A.; Hutchison, J. E.; Murray, R.; Fosset, B.; Amatore, C. Interdigitated Array Electrode as an Alternative to the Rotated Ring−Disk Electrode for Determination of the Reaction Products of Dioxygen Reduction. *Anal. Chem.* **1996**, *68* (17), 2951−2958.
(38) Liu, F.; Kolesov, G.; Parkinson, B. A. Preparation, Applications, and Digital Simulation of Carbon Interdigitated Array Electrodes. *Anal. Chem.* **2014**, *86* (15), 7391−7398.
(39) Hu, M.; Fritsch, I. Application of Electrochemical Redox Cycling: Toward Differentiation of Dopamine and Norepinephrine. *Anal. Chem.* **2016**, *88* (11), 5574−5578.
(40) Huang, J.; Pan, B.; Duan, W.; Wei, X.; Assary, R. S.; Su, L.; Brushett, F. R.; Cheng, L.; Liao, C.; Ferrandon, M. S.; Wang, W.; Zhang, Z.; Burrell, A. K.; Curtiss, L. A.; Shkrob, I. A.; Moore, J. S.; Zhang, L. The Lightest Organic Radical Cation for Charge Storage in Redox Flow Batteries. *Sci. Rep* **2016**, *6* (1), 32102.
(41) Robinson, S. G.; Yan, Y.; Hendriks, K. H.; Sanford, M. S.; Sigman, M. S. Developing a Predictive Solubility Model for Monomeric and Oligomeric Cyclopropenium-Based Flow Battery Catholytes. *J. Am. Chem. Soc.* **2019**, *141* (26), 10171−10176.
(42) Luo, J.; Hu, M.; Wu, W.; Yuan, B.; Liu, T. L. Mechanistic Insights of Cycling Stability of Ferrocene Catholytes in Aqueous Redox Flow Batteries. *Energy Environ. Sci.* **2022**, *15* (3), 1315−1324.
(43) Fan, F.-R. F.; Kwak, J.; Bard, A. J. Single Molecule Electrochemistry. *J. Am. Chem. Soc.* **1996**, *118* (40), 9669−9675.
(44) Ciolkowski, E. L.; Cooper, B. R.; Jankowski, J. A.; Jorgenson, J. W.; Wightman, R. M. Direct Observation of Epinephrine and Norepinephrine Cosecretion from Individual Adrenal Medullary Chromaffin Cells. *J. Am. Chem. Soc.* **1992**, *114* (8), 2815−2821.
(45) Beiginejad, H.; Nematollahi, D.; Varmaghani, F.; Bayat, M. Efficient Factors on the Hydrolysis Reaction Rate of Some P *Ara* -Aminophenol Derivatives in Acidic PHs. *J. Electrochem. Soc.* **2013**, *160* (8), H469−H473.
(46) Hawley, D.; Adams, R. N. Homogeneous Chemical Reactions in Electrode Processes: Measurement of Rates of Follow-up Chemical Reactions. *J. Electroanal. Chem. 1959* **1965**, *10* (5), 376−386.
(47) Menezes, H. A.; Maia, G. Films Formed by the Electro-oxidation of P-Aminophenol (p-APh) in Aqueous Medium: What Do They Look Like? *J. Electroanal. Chem.* **2006**, *586* (1), 39−48.
(48) Sun, T.; Blanchard, P.-Y.; Mirkin, M. V. Cleaning Nano-electrodes with Air Plasma. *Anal. Chem.* **2015**, *87* (8), 4092−4095.
(49) Sevov, C. S.; Samaroo, S. K.; Sanford, M. S. Cyclopropenium Salts as Cyclable, High-Potential Catholytes in Nonaqueous Media. *Adv. Energy Mater.* **2017**, *7* (5), 1602027.
(50) Fenton, A. M.; Jha, R. K.; Neyhouse, B. J.; Kaur, A. P.; Dailey, D. A.; Odom, S. A.; Brushett, F. R. On the Challenges of Materials and Electrochemical Characterization of Concentrated Electrolytes for Redox Flow Batteries. *J. Mater. Chem. A* **2022**, *10*, 17988.

https://doi.org/10.1021/acsmeasuresciau.2c00054
ACS Meas. Sci. Au 2023, 3, 62−72